Solar Energy Materials & Solar Cells 117 (2013) 638–644

Contents lists available at ScienceDirect

Solar Energy Materials & Solar Cells

journal homepage: www.elsevier.com/locate/solmat

Effects of quantum dot charging on photoelectron processes and solar cell characteristics

Kimberly A. Sablon [a,*], Andrei Sergeev [b], Nizami Vagidov [b,c], John W. Little [a], Vladimir Mitin [b]

[a] U.S. Army Research Laboratory, 2800 Powder Mill Road, Adelphi, MD 20783, United States
[b] University at Buffalo, The State University of New York, Buffalo, NY 14260, United States
[c] Optoelectronic Nanodevices LLC, Amherst, NY 14226, United States

ARTICLE INFO

Available online 2 November 2012

Keywords:
Quantum dot solar cell
IR harvesting
Selective doping
Potential barrier

ABSTRACT

We present theoretical and experimental analysis of photocarrier kinetics in quantum dot (QD) solar cells. The measurements of the *J–V* characteristics reveal strong effects of QD charging by selective doping of the interdot space on the solar cell characteristics. We demonstrate that charging of QDs significantly increases electron coupling to sub-bandgap photons, provides effective harvesting of IR energy, and serve as an effective tool for manipulating the potential profile at the micro- and nanoscale. The potential well for electrons in InAs QDs is substantially deeper than that for holes and, due to major differences between the effective masses of electrons and holes, the electron level spacing is substantially larger than the level spacing for holes. Therefore, QDs act as deep traps for electrons but shallow traps for holes. Filling of QDs under illumination is determined by a condition of equality of electron and hole capture rates which is realized via strong exponential dependence of the capture rates on the potential barrier around a charged dot. Without adequate doping of the QD medium, QDs are filled by electrons from the n-doped junction area and deteriorate the solar cell performance. However, selective n-doping of the QD medium results in micro- and nanoscale potential profiles favorable for photovoltaic conversion. Potential barriers around charged QDs decrease the photoelectron capture processes and suppress recombination processes via QDs. The filling of QDs predominantly from dopants in the QD medium allows one to maintain the microscale potential profile analogous to that in the best conventional single-junction solar cells.

1. Introduction

Photovoltaic conversion is expected to be the most cost competitive technology for off-grid (remote) commercial, industrial, and military applications. To achieve the competitive cost of a few cents per kW h, either a solar cell with moderate efficiency of $\sim 10\%$ should have a low cost of $\sim \$10/m^2$ or a solar cell with high efficiency of $\sim 50\%$ should have a moderate cost of $\$100/m^2$. Various concepts for achieving high efficiency photovoltaic conversion have attracted much attention in the scientific and engineering communities for many years. The maximum theoretical efficiency for conversion of unconcentrated solar radiation that can be achieved in conventional single-junction solar cells is given by the Shockley–Queisser limit, which is 31% for AM0 spectrum [1]. This fundamental limitation in conversion arises from the relaxation to band-edges of photocarriers that are produced by photons with energies above the bandgap and by the cut-off of all photons with energies below the bandgap (see Fig. 1). To obtain a photovoltaic efficiency above the Shockley–Queisser limit, the electron levels should be adjusted to the energy of incoming photons.

The most developed concept for high efficiency photovoltaic conversion is a multi-junction solar cell with a set of junctions having different bandgaps. The junction with the largest bandgap is placed on the top and other junctions are placed in the order of decreasing bandgaps, such that each junction absorbs and converts the photons with energies between its own bandgap and that of the previous junction. Even two–three junction cells are expected to allow for significant reduction of the thermalization losses: efficiencies of 55.9% and 63.8% can be reached, with two- and three-junction cells, respectively. For high concentration of solar energy and an infinite number of junctions the limiting efficiency is 86% [3]. However, current technology enables only triple-junction cells. This technological limitation is due to differences in the thermal expansion of materials, matching requirements of lattice constants as well as the current in a cascade of junctions [4]. The

* Corresponding author. Tel.: +1 301 394 5741.
E-mail address: ksablon@gmail.com (K.A. Sablon).

0927-0248/$ - see front matter © 2012 Elsevier B.V. All rights reserved.
http://dx.doi.org/10.1016/j.solmat.2012.10.002

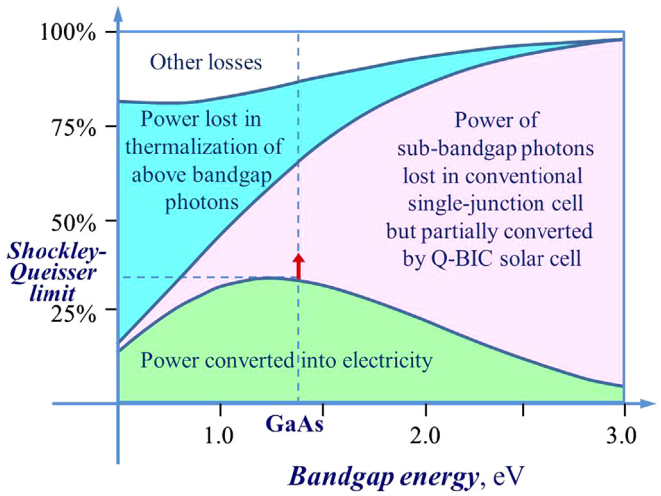

Fig. 1. Usable power, thermalization losses, and losses of sub-bandgap photons as a function of the bandgap in a single-junction solar cell. The Q-BIC technology allows for conversion of sub-bandgap photons. 5% increase (red arrow) in efficiency due to sub-bandgap photons has been already demonstrated [2]. (For interpretation of the references to color in this figure caption, the reader is referred to the web version of this article.)

maximum conversion efficiency for unconcentrated radiation realized in triple-junction cells is ~34% [5], which is just slightly above the Shockley–Queisser limit for a single-junction cell.

However, the potential to increase the photovoltaic efficiency by adding extra energy levels in a single-junction device gained footing since the early sixties when Wolf proposed to use impurities to create a midgap subband for collecting long-wavelength radiation via two-step electron transitions [6]. In addition to band–band transitions in conventional solar cell, the electron–hole pairs in this device may be generated in a two-step process. Electron is excited from the valence band to the midgap subband by the first photon and another carrier is excited from the subband to the conduction band by a second photon. A maximum efficiency of 62.3% can be achieved with an optimized position of the impurity subband which is almost identical to the theoretically predicted efficiency of a three-junction tandem solar cell. However, formation of the impurity subband has undesirable and inevitable consequences. The presence of impurities drastically enhances the Shockley–Read–Hall recombination, which deteriorates the device performance. Keevers and Green performed detailed calculations and concluded that in the optimized impurity solar cell the conversion efficiency may increase by 1–2% absolute [7]. They highlighted that the impurities can provide substantial harvesting of sub-bandgap photons and increase the short circuit current by ~5 mA/cm^2. However, at high voltages impurities become effective recombination centers and always reduce the open-circuit voltage. Trade-off between IR energy harvesting and recombination losses due to impurities is a long-term problem studied without noticeable success in a number of theoretical and experimental investigations. To date, no laboratory cell that improves efficiency due to impurities has been shown and confirmed.

The modern version of the impurity solar cell is the quantum dot (QD) intermediate band solar cell. In this device the intermediate band is formed from discrete QD levels due to strong tunnel coupling between QDs [8,9]. Improvement in the photovoltaic conversion in QD intermediate band solar cell was expected due to specific photocarrier kinetics with the multiple exciton generation, which may reduce the relaxation losses related to electron–phonon processes [10,11]. To put this concept into practice, a number of technological problems should be solved. Formation of the intermediate band from discrete QD levels requires QDs of the same size and shape. Also, QD layers should be placed at regular positions in the structure. The correlated positions of QDs are realized due to local stress transferred from one QD layer to another. However, increasing the number of closely placed QD layers above 10–15 may degrade the performance of the device due to critical accumulation of strain which in turn reduces the carrier mobility. Thus far, intensive technological efforts to improve intermediate band solar cell show very limited success and an increase in the photovoltaic efficiency due to addition of QDs does not exceed 1% [12].

2. Photocarrier kinetics in Q-BIC structures

Quantum dots are multi-functional and scalable nanoblocks, which allow for fabrication of nanomaterials with specific optical and electrical properties favorable for photovoltaic conversion [13,14]. Is the formation of the intermediate band necessary to employ unique opportunities of QD nanomaterials for photovoltaic harvesting and conversion? Not at all! Besides band engineering, quantum dots provide effective ways for the engineering of 3D nanoscale potential profile to control photocarrier processes. To form the nanoscale potential profile favorable for photovoltaic applications, we propose to employ *q*uantum dots with *b*uilt-*in* *c*harge (Q-BIC), where QDs are charged via selective doping of the interdot space [2,15]. Charged dots create local potential barriers around single dots and collective potential barriers around dot clusters, rows, and other dot groups. Such potential barriers effectively separate QDs or QD areas, where harvesting of sub-bandgap photons is realized, from conducting channels where the photovoltaic conversion takes place. As in the case of impurity solar cells, the key problem of conventional QD photovoltaic materials is the enhanced recombination via additional energy levels which are introduced by QDs. In Q-BIC nanomaterials, the capture of photoelectrons into QDs is strongly suppressed by charging of QDs. Suppression of photoelectron capture directly increases the photoelectron lifetime and decreases the recombination losses. To suppress the photocarrier capture by potential barriers, the barrier height should be 2–3 times larger than k_BT. Therefore, at room temperatures, the local barriers should be at least 0.05 eV and QDs comprise at least 5–10 electrons. This requires relatively large dots and substantial doping of the interdot space.

To apply the Q-BIC technology for managing bipolar kinetics of photoelectrons and holes, it is important to determine which carriers are captured first and suppress these fast capture processes. The difference between electron and hole capture processes is mainly determined by the structures of electron and hole energy levels. The level structure in InAs/GaAs QD materials has been investigated in numerous photoluminescence measurements. All data show practically equidistant level positions of electrons and holes [15–20], as shown in Fig. 2. The total level spacing, $\Delta E = \Delta E_e + \Delta E_h$, which is directly determined in photoluminescence experiments, was found to be 60–80 meV [15–20]. The ratio, $\Delta E_e/\Delta E_h$, is evaluated indirectly from various measurements and found to be from 2 to 8 [15–17]. In our opinion, the specific equidistant positions of energy levels may be associated with the quasi-parabolic form of the confinement potential in InAs/GaAs QDs. In this model, the spacing ratio, $\Delta E_e/\Delta E_h$, is given by $(m_h/m_e)^{1/2} \approx 4$, which is in reasonable agreement with the scope of the experimental results. Using this model we obtained: $\Delta E_e \approx 55$ meV and $\Delta E_h \approx 14$ meV. Therefore, the electron transitions in QDs significantly exceed the thermal energy and cannot be induced by thermal phonons, while the hole transitions are induced by acoustic thermal phonons. Thus, to stimulate electron

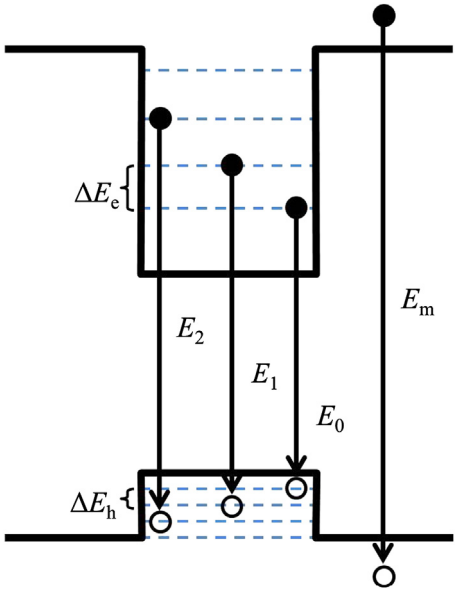

Fig. 2. Energy levels structure in InAs/GaAs quantum dots. The total level spacing $\Delta E = \Delta E_e + \Delta E_h = 60-80$ meV; the electron level spacing is substantially larger than that for holes: $\Delta E_e/\Delta E_h \approx 4$.

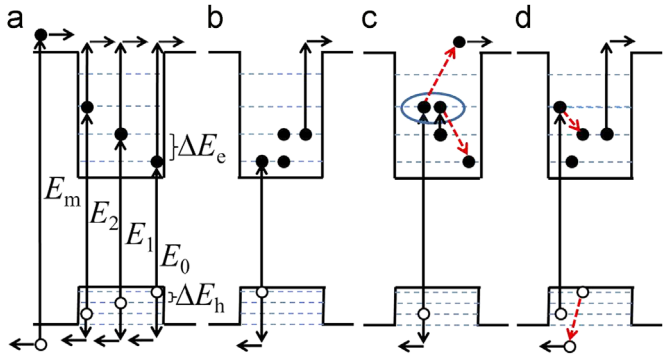

Fig. 3. IR-assisted photogeneration of electron–hole pairs in undoped QD structures (a) and n-doped QD structures (b–d). Processes (c) and (d) are realized via e–e and e–h interaction. (For interpretation of the references to color in this figure caption, the reader is referred to the web version of this article.)

transitions by IR radiation for photovoltaic applications, n-doping is strongly preferred.

Fig. 3 shows the IR-assisted photogeneration of electron and hole pairs in undoped (Fig. 3(a)) and n-doped InAs/GaAs QD structures (Fig. 3(b)–(d)). Fig. 3(b) describes a two-step process induced by n-doping with IR transition of electron from the localized to the conducting state. Fig. 3(c) and (d) shows other n-doping induced processes that involve inter-electron interaction in QDs. In Fig. 3(c) the radiation excites two electrons to QD excited states, then one of these electrons transfers to the conducting state and the other transfers to a low-energy state. In Fig. 3(d) the relaxation of electron to a low-energy state leads to the escape of a hole from the QD. We would like to highlight that, because of the small hole level spacing, the hole escape from QDs can be easily generated by hot (excited) electrons. Thus, doping should stimulate the radiation-induced electron escape from QDs. Therefore, in contrast to the lasing applications of QDs, which require strong p-doping of the active medium, for the photovoltaic devices only n-doping of the QD medium is desirable.

Along with the enhancement of photoinduced electron escape from QDs, the n-doping also suppresses the capture of photoelectrons due to the potential barriers around QDs. Suppression of photoelectron capture processes is also very favorable for photovoltaic applications, because in InAs/GaAs QD structures the capture of electrons is substantially faster than the capture of holes. Let us note that in bulk GaAs or InAs materials, the hole relaxation via emission of optical phonons is faster than the corresponding electron relaxation, but the hierarchy of capture processes in undoped and weakly doped QD structures is exactly opposite [21–24]. This is directly related to the level structure of QDs. Because the hole level spacing is smaller than the thermal energy, the hole trapping has a cascade mechanism, which may be described in terms of hole diffusion over energy levels. Such capture with back and forth motion through multiple levels is substantially slower than the capture via high energy optical phonons.

In Table 1, where N is the electron dot population, FF is the fill factor, and η is the efficiency of solar cell, we summarize photovoltaic characteristics of our Q-BIC solar cells with the built-in charge up to six electrons per dot [2]. As seen, an increase in the built-in-dot charge results in the increase in the short-circuit current, J_{SC}, from 15.1 mA/cm^2 to 24.3 mA/cm^2, practically without degradation of the open-circuit voltage, V_{OC}. We have not observed any evidence of saturation of the effect and, therefore, even higher efficiencies are anticipated for higher doping.

Let us note that the investigated Q-BIC test devices were relatively short (~ 1.4 μm) and did not have antireflection coating and back surface field barriers. As a result, the efficiency of our reference cell (without QDs) was substantially less than the record efficiencies of GaAs cells. At the same time, our data demonstrate very effective harvesting and conversion of IR radiation by charged dots. The third column in Table 1, J_{SC}^{IR}, shows the IR contribution to the short-circuit current. We would like to highlight that J_{SC}^{IR} has been independently and directly measured in experiments, where the absorption of the short-wavelength part of solar spectrum was completely suppressed by the corresponding GaAs filter. As seen from Table 1, the conversion of IR radiation increases with the increase of the built-in-dot charge. At the n-doping which provides six electrons per dot, the conversion of solely IR radiation via QD transitions gives ~ 9 mA/cm^2 contribution to the short circuit current. Thus, in these Q-BIC test devices the harvesting and conversion of the IR part of solar spectrum give an additional 5% to the photovoltaic efficiency (see Fig. 1). Charging of quantum dots provides an effective tool for managing photocarrier processes and the potential profile. As we discussed above, for effective harvesting of sub-bandgap photons and suppression of recombination processes via QDs, n-charged QDs are strongly preferred. Below we consider the effect of dot charging on electron processes in Q-BIC structures.

2.1. The photoelectron capture by repulsive n-charged QDs

The photoelectron capture by the repulsive charged QD may be realized either via tunneling through the barrier or by thermal excitation above the barrier. Let us first evaluate the relative probability of these two processes for a simple model of a spherical dot of radius a. The probability of tunneling reaches a maximum for an electron moving along the dot radius. For electron with

Table 1
Q-BIC solar cell parameters vs dot charge [2].

N (el/dot)	J_{SC} (mA/cm^2)	J_{SC}^{IR} (mA/cm^2)	V_{OC} (V)	FF (%)	η (%)
Ref. cell	14.6	0	0.81	80	9.07
0	15.1	4.1	0.77	77	9.31
2	17.3	7.2	0.74	76	9.73
3	18.5	8.1	0.79	75	12.1
6	24.3	9.3	0.78	72	14.0

energy ε, this probability is proportional to $\exp[-2\pi(E_B/\varepsilon)^{1/2}]$ where E_B is the Bohr energy, $E_B = 2\pi^2 N^2 e^4 m/(h^2\kappa)$, N is the number of electrons captured in a dot, m is the electron mass, and κ is the permittivity. Then, in the case of the Boltzmann distribution of photocarriers, the tunneling probability is proportional to $[-2\pi(E_B/\varepsilon)^{1/2} - \varepsilon/k_BT]$. The characteristic energy of tunneling particles is given by $\varepsilon^* = [E_B(\pi k_B T)^2]^{1/3}$. The characteristic spatial scale is determined by the turning point for the tunneling under the Coulomb barrier: $r^* = Ne^2/(\kappa\varepsilon^*)$. For the electron with the energy ε^* we have

$$r^* = \left[\frac{2N}{\pi^2\kappa}\frac{\hbar^2}{e^2 m}\left(\frac{e^2}{k_B T}\right)^2\right]^{1/3}. \quad (1)$$

Evaluating Eq. (1) for $N \sim 5$, we get $r^* \sim 5$ nm at a room temperature. If characteristic dot size, a, is smaller than r^*, the tunneling processes dominate in the photoelectron capture. In this case, the temperature dependence of the capture rate is expected to be the same as for the repulsive impurity centers [25],

$$\frac{1}{\tau_{capt}} \propto \exp\left[-\left(\frac{27\pi^2 E_B}{k_B T}\right)^{1/3}\right]. \quad (2)$$

In the opposite case, $r^* > a$, the thermal activated processes dominate over tunneling and the electron capture rate, τ^e_{capt}, is expected to follow the exponential dependence [26]:

$$\frac{1}{\tau^e_{capt}} = \pi N_d a^3 \tau_\varepsilon^{-1} \exp\left[-\frac{Ne^2}{k_B T\kappa a}\right] \quad (3)$$

where N_d is the dot concentration, τ_ε is the inelastic scattering time which corresponds to transitions with characteristic QD spacing due to electron interaction with optical phonons. Usually in QD structures the characteristic dot size is comparable or larger than r^*. Therefore, in contrast to the capture by the repulsive impurity centers, the capture rate by charged QDs exponentially depends on the height of potential barriers,

$$V = \frac{Ne^2}{\kappa a}. \quad (4)$$

2.2. Cascade hole capture by n-charged QDs

The characteristic spatial scale in the repulsive Coulomb potential is given by Thomson's radius for $\varepsilon = k_BT$,

$$R_{Th} = \frac{Ne^2}{k_B T\kappa}. \quad (5)$$

Therefore, for QD structures the characteristic scale, R^*, is $\max\{R_{Th}, a\}$ and Thomson's capture rate is

$$\frac{1}{\tau^h_{capt}} = \frac{4}{3}\pi N_d (R^*)^3 \tau_\varepsilon^{-1}. \quad (6)$$

Notice that because of the different level spacing, the corresponding relaxation mechanisms for electron and holes are completely different. The hole relaxation between levels is determined by thermal acoustic phonons. Keeping in mind that the hole level spacing E_h is smaller than k_BT, the inelastic relaxation rate in Eq. (6) may be evaluated as $\tau_0(k_BT/\Delta E_h)$, where τ_0 is the relaxation time between adjacent hole levels.

2.3. Inter-electron interaction in QDs

Carrier confinement in small volume of QDs provides strong interaction between carriers. In particular, this leads to multi-exciton generation in QDs, which is important for photovoltaic applications [18]. The relaxation processes highlighted in red in Fig. 3(c) and (d) are also very favorable for photovoltaic applications.

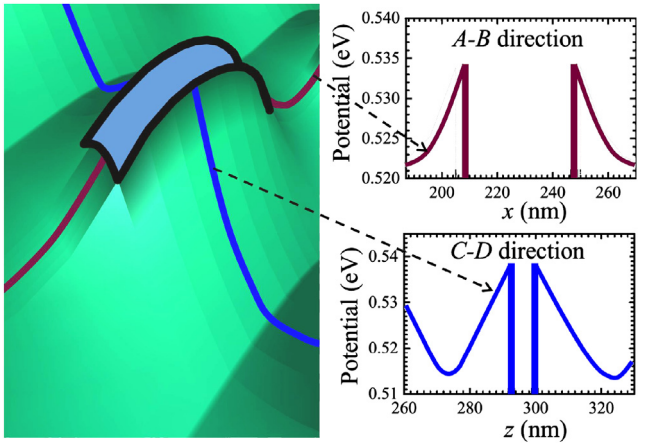

Fig. 4. Truncated pyramidal QD: potential barriers in longitudinal (A–B-direction) and perpendicular direction (C–D-direction) are two times smaller.

2.4. Effects of QD shape

The potential barriers around realistic QDs are strongly anisotropic. Fig. 4 shows the potential profile calculated employing nextnano3 software [27]. As seen from Fig. 4, the potential barriers around QDs in the form of truncated pyramids are strongly asymmetric. The barriers in the QD planes, i.e. in the A–B direction which is perpendicular to the current, are substantially smaller than the barriers in the direction of the current C–D direction. Therefore, electron trapping is effective for electrons moving along the A–B direction. A percentage of such electrons decreases in structures with vertically correlated positions of QDs, where electrons move mainly in the channels between dots (Fig. 4).

Comparing trapping rates of electrons and holes, i.e. Eqs. (3) and (6), let us note that in the bulk materials the inelastic electron relaxation time, τ_ε, is shorter than the one for holes. However, the exponential factor in Eq. (3) can drastically decrease the electron capture rate. Moreover, in stationary conditions under sunlight, the electron and hole capture rates are equated by changing of the electron filling of the dots. In "underdoped" structures QDs will be filled by photoelectrons, but in "overdoped" structures electrons will leave the QDs. Therefore, to optimize the potential profile in QD solar cells, one should choose the optimal doping that provides equal electron and hole capture rates, i.e. $\tau^e_{capt}(N) = \tau^h_{capt}(N)$ where the electron filling of QDs, N, corresponds to the doping, i.e. a number of dopants per dot.

3. Dark J–V characteristics of Q-BIC structures

To understand the electron processes in our Q-BIC structures, we investigated the dependencies of the dark J–V characteristics on the built-in-dot charge.

The evaluated solar cell structures were grown by molecular beam epitaxy (MBE) on n^+-GaAs (100). The structures consisted of 20 layers of InAs/GaAs QDs with a lateral size of 30 nm and average height of 3.6 nm spaced by a 50 nm thick GaAs layer. The thickness of the GaAs spacer layer was chosen to dissipate strain accumulation from one layer to the next. The QD solar cells were delta-doped in the middle of the GaAs spacer layers that separated layers with QDs with Si and Be for n- and p-doping, respectively. The dopant sheet density was varied to provide zero, two, three, four, and six electrons per dot. Further details of the growth and fabrication processes have been described elsewhere [2,15,28].

The current–voltage characteristics of our devices were measured in the range of 296–400 K using a thermoelectric Peltier cooler/heater connected to a Hewlett-Packard 6651A power supply. A temperature probe was used for monitoring the temperature. The data for devices with selective n-doping that provides zero, two, three, four, and six electrons per dot, for a device with p-doping that provides four holes per dot, and for the reference cell without QDs are presented in Fig. 5(a)–(c) for the following temperatures: 296 K (Fig. 5(a)), 340 K (Fig. 5(b)), and 380 K (Fig. 5(c)). As seen, the dark current in the undoped QD device is two orders of magnitude higher than that in the reference cell. The p-doping of QD device also significantly increases the dark current and deteriorates the device performance, while in the n-doped devices the increase in the dark current is substantially smaller.

The data obtained were analyzed in the framework of the diode model [29] in terms of the ideality factor, n, the diode saturation current density, J_0, the shunt resistance, R_{SH}, and the series resistance, R_{SR}:

$$J = J_0\left[\exp\left(\frac{e(V-JR_{SR})}{nk_BT}\right)-1\right]+\frac{V-JR_{SR}}{R_{SH}}. \quad (7)$$

The diode ideality factor, n, is a characteristic of the recombination–generation (G-R) processes in the device regions where the voltage-induced nonequilibrium carrier kinetics takes place. As it is known, $n=1$ corresponds to the radiative G-R processes in the charge-neutral regions, $n=2$ is associated with the G-R via midgap traps (the Shockley–Read–Hall recombination). QDs provide intensive G-R processes via quantum dot levels. Usually, generation–recombination via QDs strongly increases the ideality factor up to 3 and more [30].

To obtain the ideality factor from J–V curves presented in Fig. 5, let us note that at high voltages, $V \gg k_BT/e = 25$ mV, the J–V curves are described by an exponential dependence, from which the ideality factor, n, may be directly calculated. The ideality factor for our GaAs reference cell turns out to be practically independent on voltage and temperature and it is equal to $n \approx 1.7$ which is close to the values obtained in other works [31].

The voltage dependencies of the ideality factor of QD devices are presented in Fig. 6. As seen, in the undoped quantum dot solar cells the ideality factor strongly depends on voltage, while in the n-doped samples the ideality factor just slightly changes with voltage. In the undoped device at low voltages (below 0.35 V) and at high voltages (above 0.8 V) the ideality factor exceeds 3. This demonstrates that in this device the filling of QDs significantly changes with biased voltage and at high and low voltages QD contribution to G-R processes dominates over radiative and Shockley–Read–Hall G-R processes. As we discussed in Section 2, the electron energy level spacing is substantially larger than the spacing for holes and thermal energy. Therefore, the electrons are captured substantially faster than holes and this leads to the accumulation of electron charge in QDs from the n^+-pre-contact area. A process of the charge accumulation by QDs saturates, when electron capture rate becomes equal to that for holes due to potential barriers around QDs created by the accumulated charge. Naturally, the charge redistribution in the undoped device strongly depends on the applied voltage.

In the n-doped devices, the ideality factor is close to 2. In the device with maximal doping of six electrons per dot, the ideality factor weakly decreases with voltage increase from $n \approx 2.5$ at 0.4 V to $n \approx 1.7$ at 0.9 V. Thus, at characteristic voltages, $V \sim V_{OC}$, the ideality factor of strongly doped cell is close to that in the reference cell. Also, the n-doping of QD medium suppresses

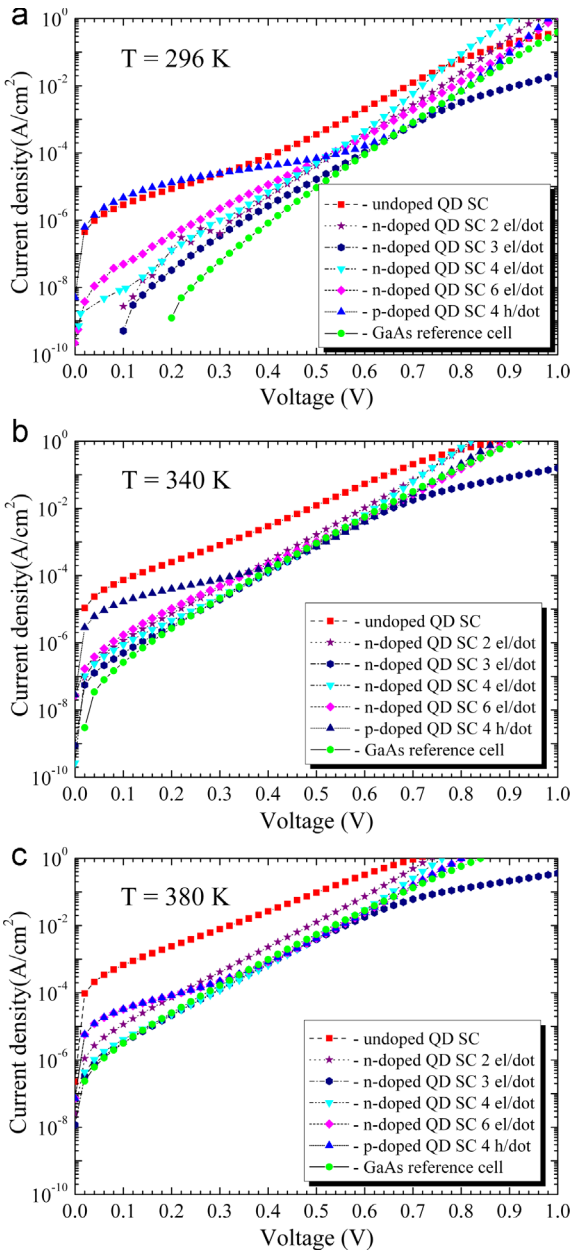

Fig. 5. Measured dark current densities in GaAs reference cell, undoped QD solar cell, p-doped (four holes per dot) QD solar cell, and n-doped (two, three, four, and six electrons per dot) QD solar cells at 296 K (a), 340 K (b), and 380 K (c).

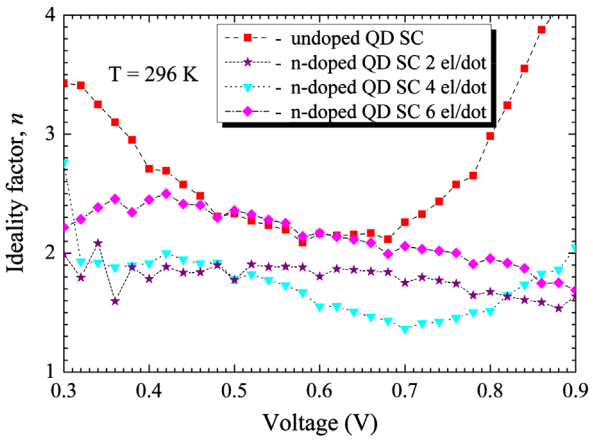

Fig. 6. Calculated from dark current measurements ideality factor dependences on applied voltage of undoped QD solar cell and n-doped (two, four, and six electrons per dot) QD solar cells. T=296 K.

unwanted charge redistribution between QD region and the pre-contact area.

Like the voltage dependencies, the temperature dependencies of the ideality factor in the n-doped devices are substantially weaker than that in the undoped device. In particular, in the undoped device the low-voltage ideality factor changes from $n \approx 3.2$ at 296 K to $n \approx 2.4$ at 380 K. For the n-doped solar cells with two electrons per dot, the ideality factor changes from $n \approx 1.8$ at 296 K to $n \approx 1.7$ at 380 K. For the n-doped solar cells with six electrons per dot, the ideality factor decreases from $n \approx 2.4$ at 296 K to $n \approx 2.1$ at 380 K.

The saturation diode current density, J_0, was directly obtained from a pre-factor in the exponential voltage dependence of the dark current. The temperature dependencies of the saturation current in our devices are presented in Fig. 7. For all devices, J_0 shows an exponential temperature dependence, $J_0 = J_{00} \exp(-\Delta/k_B T)$. As it is expected, for the GaAs reference cell the activation energy, Δ, determined from Fig. 7, corresponds to the GaAs bandgap of 1.4 eV. The saturation current in the undoped QD solar cell is more than two orders of magnitude higher than that in the n-doped samples. This evidences in favor of strong charge accumulation in QDs from pre-contact area and substantial changes in the microscale potential profile due to this charge redistribution. The saturation current in the n-doped devices with two and three electrons per dot is close to that in the GaAs reference cell. In the n-doped device with six electrons per dot the saturation current density increases, but it is still substantially less than that in the undoped devices. In all QD devices, the activation energy weakly depends on doping and its value changes from ~ 0.7 eV at 296 K to ~ 1 eV at 380 K. This observation shows that G-R processes in all QD devices involve the same QD energy levels, but their intensity strongly depends on the potential profile that is created after the electron density redistribution between QDs and pre-contact area.

The shunt resistance, R_{SH}, for all samples was sufficiently high to ensure losses due to shunt currents to be below 1% of the output power. R_{SH} for n-doped devices and reference was in the range of 1 GΩ, while for undoped devices it was two orders of magnitude smaller.

Summarizing this section, we would like to highlight that insufficient doping of QD medium leads to the significant charge redistribution between QD medium and pre-contact area, which deteriorates the device performance. This effect is illustrated by Fig. 8, which shows the potential profiles at low current injection in the conventional GaAs single-junction solar cell, the n-doped QD solar cell with six electrons per dot, and the undoped QD solar cell. As seen, the n-doping of QD medium provides the potential

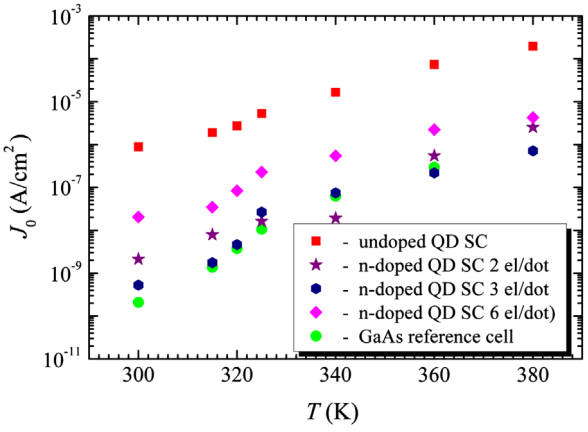

Fig. 7. Calculated from dark current measurements saturation current density dependences on temperature of GaAs reference cell, undoped QD solar cell, and n-doped (two, four, and six electrons per dot) QD solar cells.

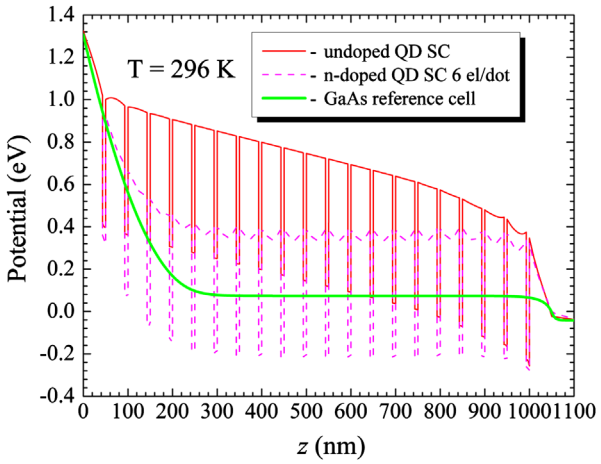

Fig. 8. Calculated potential profiles in *C–D* direction of undoped, n-doped (six electrons per dot) QD solar cells and GaAs reference cell.

distribution similar to the conventional single junction solar cell. Because the space-charge region plays the role of a membrane that separates electrons and holes [32], such profile with narrow space-charge region is strongly favorable for effective conversion. In the undoped QD solar cell, the potential slowly changes in the wide area that prevents effective photovoltaic conversion.

4. Conclusions

Our theoretical analysis and measurements of dark *J–V* characteristics demonstrate strong effects of selective doping of QD medium on the micro- and nanoscale potential profile in QD photovoltaic devices. Charging of QDs enhances harvesting of IR radiation and suppresses the recombination losses due to nanoscale potential barriers around QDs. Adequate doping of QD medium also prevents the charge redistribution between the QD medium and pre-contact area and provides the microscale potential distribution favorable for effective photovoltaic conversion.

Acknowledgments

The authors would like to thank Dr. Stefan Birner from Walter Schottky Institut, Technische Universität München for valuable advices on 3D modeling of QD devices.

This work was partially supported by Air Force Office of Scientific Research (AFOSR). The research of A.S. was also supported by the NSF DMR under Grant no. 0907126. The research of N.V. was supported by NSF SBIR under Grant no. 1215033.

References

[1] W. Shockley, H.J. Queisser, Detailed balance limit of efficiency of p-n junction solar cells, Journal of Applied Physics 32 (1961) 510–519.
[2] K.A. Sablon, J.W. Little, V. Mitin, A. Sergeev, N. Vagidov, K. Reinhardt, Strong enhancement of solar cell efficiency due to quantum dots with built-in charge, Nano Letters 11 (2011) 2311–2317.
[3] M.A. Green, Third Generation Photovoltaics, Springer-Verlag, Berlin, Heidelberg, 2006.
[4] M. Yamaguchi, T. Takamoto, K. Araki, N. Ekins-Daukes, Multi-junction III–V solar cells: current status and future potential, Solar Energy 79 (2005) 78–85.
[5] M.A. Green, K. Emery, Y. Hishikawa, W. Warta, E.D. Dunlop, Solar cell efficiency tables (version 39), Progress in Photovoltaics: Research and Applications 20 (2012) 12–20.
[6] M. Wolf, Limitations and possibilities for improvement of photovoltaic solar energy converters: considerations for Earth's surface operation, Proceedings of the IRE 48 (1960) 1246–1263.
[7] M.J. Keevers, M.A. Green, Efficiency improvements of solar cells by the impurity photovoltaic effect, Journal of Applied Physics 75 (1994) 4022–4031.

[8] A. Luque, A. Martí, The intermediate band solar cell: progress toward the realization of an attractive concept, Advanced Materials 22 (2010) 160–174.
[9] A.J. Nozik, Nanoscience and nanostructures for photovoltaics and solar fuels, Nano Letters 10 (2010) 2735–2741.
[10] R.D. Schaller, V.I. Klimov, High efficiency carrier multiplication in PbSe nanocrystals: implications for solar energy conversion, Physical Review Letters 92 (2004) 186601-1–186601-4.
[11] M.C. Beard, A.G. Midgett, M.C. Hanna, J.M. Luther, B.K. Hughes, A.J. Nozik, Comparing multiple exciton generation in quantum dots to impact ionization in bulk semiconductors: implications for enhancement of solar energy conversion, Nano Letters 10 (2010) 3019–3027.
[12] D. Guimard, R. Morihara, D. Bordel, K. Tanabe, Y. Wakayama, M. Nishioka, Y. Arakawa, Fabrication of InAs/GaAs quantum dot solar cells with enhanced photocurrent and without degradation of open circuit voltage, Applied Physics Letters 96 (2010) 203507-1–203507-3.
[13] K. Tanaba, K. Watanabe, Y. Arakawa, Flexible thin-film InAs/GaAs quantum dot solar cells, Applied Physics Letters 100 (2012) 192102-1–192102-3.
[14] X.-J. Shang, J.-F. He, M.-F. Li, F. Zhan, H.-Q. Ni, Z.-C. Niu, H. Pettersson, Y. Fu, Quantum-dot-induced optical transition enhancement in InAs quantum-dot-embedded p-i-n GaAs solar cells, Applied Physics Letters 99 (2011) 113514-1–113514-3.
[15] K.A. Sablon, J.W. Little, V. Mitin, A. Sergeev, N. Vagidov, Solar cell with built-in charge: experimental studies of diode model parameters, Journal of Vacuum Science and Technology A 30 (2012) 04D104-1–04D104-4.
[16] K.H. Schmidt, G. Medeiros-Ribeiro, M. Oestreich, P.M. Petroff, G.H. Döhler, Carrier relaxation and electronic structure in InAs self-assembled quantum dots, Physical Review B 54 (1996) 11346–11353.
[17] M.J. Steer, D.J. Mowbray, W.R. Tribe, M.S. Skolnick, M.D. Sturge, M. Hopkinson, A.G. Cullis, C.R. Whitehouse, R. Murray, Electronic energy levels and energy relaxation mechanisms in self-organized InAs/GaAs quantum dots, Physical Review B 54 (1996) 17738–17744.
[18] J. Siegert, S. Marcinkevičius, Q.X. Zhao, Carrier relaxation and electronic structure in InAs self-assembled quantum dots, Physical Review B 72 (2005) 085316-1–085316-7.
[19] F. Adler, M. Geiger, A. Bauknecht, F. Scholz, H. Schweizer, M.H. Pilkuhn, B. Ohnesorge, A. Forchel, Optical transitions and carrier relaxation in self assembled InAs/GaAs quantum dots, Journal of Applied Physics 80 (1996) 4019–4026.
[20] W.-H. Chang, T.M. Hsu, C.C. Huang, S.L. Hsu, C.Y. Lai, N.T. Yeh, T.E. Nee, J.-I. Chyi, Photocurrent studies of the carrier escape process from InAs self-assembled quantum dots, Physical Review B 62 (2000) 6959–6962.
[21] I.E. Itskevitch, M.S. Skolnick, D.J. Mowbray, I.A. Trojan, S.G. Lyapin, L.R. Wilson, M.J. Steer, M. Hopkinson, L. Eaves, P.C. Main, Excited states and selection rules in self-assembled InAs/GaAs quantum dots, Physical Review B 54 (1999) R2185–R2188.
[22] T. Müller, F.F. Schrey, G. Strasser, K. Unterrainer, Optical pumping as artificial doping in quantum dots-in-a-well infrared photodetectors, Applied Physics Letters 83 (2003) 3572–3574.
[23] D.A. Yarotski, R.D. Averitt, N. Negre, S.A. Crooker, A.J. Taylor, G.P. Donati, A. Stintz, L.F. Lester, K.J. Malloy, Ultrafast carrier-relaxation dynamics in self-assembled InAs/GaAs quantum dots, Journal of the Optical Society of America B 19 (2002) 1480–1484.
[24] A. Luque, A. Martí, N. López, E. Antolín, E. Cánovas, C. Stanley, C. Farmer, P. Díaz, Operation of the intermediate band solar cell under nonideal space charge region conditions and half filling of the intermediate band, Journal of Applied Physics 99 (2006) 094503-1–094503-9.
[25] V.L. Bonch-Bruevich, Concerning question of recombination of hot electrons, Soviet Physics Solid State 6 (1964) 1615–1621.
[26] A. Sergeev, V. Mitin, M. Stroscio, Quantum-dot photodetector operating at room temperatures: diffusion-limited capture, Physica B 316–317 (2002) 369–372.
[27] 〈http://www.nextnano.de/nextnano3/〉.
[28] K. Sablon, A. Sergeev, N. Vagidov, A. Antipov, J. Little, V. Mitin, Effective harvesting, detection, and conversion of IR radiation due to quantum dots with built-in charge, Nanoscale Research Letters 6 (2011) 584-1–584-13.
[29] J. Nelson, The Physics of Solar Cells, Imperial College Press, London, 2009.
[30] D. Di, I. Perez-Wurfl, A. Gentle, D.-H. Kim, X. Hao, L. Shi, G. Conibeer, M.A. Green, Impacts of post-metallisation processes on the electrical and photovoltaic properties of Si quantum dot solar cells, Nanoscale Research Letters 5 (2010) 1762–1767.
[31] S.A. Blokhin, A.V. Sakharov, A.M. Nadtochy, A.S. Pauysov, M.V. Maximov, N.N. Ledentsov, A.R. Kovsh, S.S. Mikhrin, V.M. Lantratov, S.A. Mintairov, N.A. Kaluzhniy, M.Z. Shvarts, AlGaAs/GaAs photovoltaic cells with an array of InGaAs QDs, Semiconductors 43 (2009) 514–518.
[32] P. Würfel, Physics of Solar Cells: From Basic Principles to Advanced Concepts, Wiley-VCH, Weinheim, 2005.